Kinetics of the Emulsion Polymerization of Vinylidene Fluoride and Hexafluoropropylene

Marco Apostolo and Vincenzo Arcella

Ausimont R&D, Via S. Pietro 50/A, 20021 Bollate, Milano, Italy

Giuseppe Storti and Massimo Morbidelli*

ETH Zentrum, Universitätstrasse 6, CH-8092 Zürich, Switzerland

Received April 29, 1998; Revised Manuscript Received October 10, 1998

ABSTRACT: The kinetics of emulsion polymerization of vinylidene fluoride (VDF) and hexafluoropropylene (HFP) has been investigated both experimentally and through the development of an appropriate model. Despite the practical relevance of this copolymer, information about the polymerization kinetics in the literature are rather scarce. A reasonable polymerization mechanism involves quite a number of kinetic parameters, which all need to be evaluated independently. This was obtained by running a limited number of polymerization reactions, but performing a rather accurate characterization of the polymer produced, including the polymerization rate, molecular weight, and chain end group distribution. These quantities allow for the reliable estimation of the involved kinetic parameters. The reliability of the developed model has been assessed by comparison with a second independent set of experimental data, where different operating conditions, in terms of pressure, initial concentration of the initiator, and chain-transfer agent, have been considered.

Introduction

Fluoropolymers are rather expensive polymeric materials, whose market is still growing in volume and grades because of their unique properties. Their remarkable resistance to flame, chemicals, and oxidative attack makes the fluoropolymers suitable for applications in hostile environments. A small but significant segment of fluoropolymers is represented by fluoroelastomers, characterized by a glass-transition temperature below room temperature. These are widely used when sealing capabilities in corrosive and high-temperature environments are needed, as it is often the case in the aircraft, aerospace, chemical, petroleum, and energy industries. In this work we study the kinetics of free-radical polymerization of one of these fluoroelastomers (i.e., Tecnoflon, a vinylidene fluoride(VDF)−hexafluoropropylene (HFP) copolymer industrially produced in an emulsion).

In most industrial polymerization processes, it is important to control the structure of the produced polymer chains, in particular the molecular-weight distribution (MWD), the branching frequency, and the chain end distribution. In the case of Tecnoflon, the structure of the polymeric chains determines the behavior of the polymer during the postprocessing (compression or injection molding) and the mechanical properties of the final product. Therefore, the capability of predicting the structure of the polymer is highly desirable to design a polymer matching the required characteristics. For this, one needs an appropriate mathematical model tuned on a reliable set of experimental data.

These models rely on a kinetic scheme, which should account for all the relevant chemical reactions. This is a serious problem for the system considered in this work and for fluoropolymers in general. Despite their relevance in the polymer industry, the knowledge of the chemistry of these systems is indeed incomplete, and no data are available in the open literature on the rate of the reactions involved. The first objective of this work has then been to overcome this problem by developing a detailed kinetic scheme for the copolymerization of VDF and HFP, and by providing an estimate of the kinetics of all the involved reactions. This poses an obvious problem related to the large number of reactions and then of kinetic parameters that have to be evaluated. The adopted solution is based on a rather detailed analysis of the polymer structure, which involves, besides the polymerization rate, the MWD and the chain end group distribution. The combination of all this information provides a sufficient basis for the reliable estimation of the underlying kinetic mechanism. Besides the understanding of the polymerization kinetics of the particular system under examination, the present analysis provides an example of the application of a general methodology for the complete evaluation of the kinetics of complex polymerization systems, based on a detailed characterization of the polymer structure.

On the basis of the detailed kinetic scheme mentioned above, a mathematical model able to evaluate the structure of fluorinated copolymers produced in emulsion has been developed. The molecular-weight distribution of the produced copolymer is evaluated, combining the method of moments with the numerical fractionation technique. The model is validated through the comparison with a set of experimental results of the VDF−HFP emulsion polymerization. Two reference reactions (defined base cases) have been used to estimate the kinetic parameters by fitting the model predictions to the experimental data, which involved the rate of polymerization, MWD, and chain end group distribution. Then, using the same parameter values, the capability of the model to predict the effects on the MWD of

* To whom correspondence should be addressed.

10.1021/ma980683r CCC: $18.00
Published on Web 01/27/1999

Table 1. VDF−HFP Copolymerization Reaction Recipes

run	reaction	conversion (kg/m^3)	initiator conc. (kmol/m^3)	pressure (MPa)	CTA conc. (kmol/m^3)
		Calibration Reactions			
1	14332/75	108	0.033	1.1	
2	14332/76	219	0.033	1.1	
3	14332/77	415	0.033	1.1	
4	14332/67	426	0.011	1.9	0.019
		Effect of Operating Conditions over the MWD			
5	14332/38	429	0.066	1.1	
6	14332/97	460	0.011	1.9	
7	14332/96	49	0.011	1.9	0.033
8	14332/90	101	0.011	1.9	0.033
9	14332/91	213	0.011	1.9	0.033
10	14332/92	409	0.011	1.9	0.033

operating conditions such as the reactor pressure, initiator concentration, and chain-transfer agent concentration has been investigated.

1. Experimental Section

1.1. Copolymerization Reactions. The system investigated in this work is the emulsion copolymerization of vinylidene fluoride (CH_2=CF_2, VDF) and hexafluoropropylene (CF_3CF=CF_2, HFP). Both monomers are gaseous at the following reaction conditions: temperature between 40 and 90 °C and pressure from 1 to 4 MPa. The VDF−HFP copolymer exhibits elastomeric behavior if the HFP content is larger than 20 mol %, while otherwise it is semicrystalline. The fluoropolymer under examination here is an elastomer with a composition of VDF/HFP equal to 79/21 mol %.

To understand the reaction mechanism and develop a reliable kinetic model, 10 copolymerization reactions have been carried out. In all reactions, the temperature was kept constant at 85 °C. No emulsifier is needed in these polymerizations since the latex stability is guaranteed by the ionic chain ends of the macromolecules at the particle surface. Ammonium persulfate (APS) was used as the free-radical initiator and ethyl acetate as the chain-transfer agent (CTA). The recipes of all the experiments are summarized in Table 1. Since it was difficult to collect reliable samples from the reactor during operation, the evolution of the reacting system was reconstructed by running several reactions with the same recipe and stopping them at different conversion values. This is the case for runs 1−3 and 7−10. In all cases, a gaseous monomer mixture of appropriate composition is continuously added to the reactor in order to keep the reactor pressure constant. This procedure allows the production of a copolymer with constant composition through the entire process. The first two reactions (runs 1−3 and run 4) are used to calibrate the kinetic constants of the model, while runs 5, 6, and 7−10 to verify the predictive capabilities of the model. As is apparent from Table 1, the variables changed in the recipes investigated include initiator concentration, pressure, and CTA concentration.

1.2. Experimental Apparatus. All the polymerization reactions have been carried out in a 10^{-2} m^3 pilot plant reactor (Ausimont Laboratories, Bollate, Italy) made of 316 stainless steel. It is equipped with two baffles with a width variable along the reactor axis and a stirrer with two three-bladed turbines. The typical stirring speed is 550 rpm, where transport limitations of the monomers between the gas and liquid are negligible. This has been verified by experiments (not shown here) at variable stirring speeds. The monomer mixture is fed to the reactor using a Corblin membrane pump, compressing the gas to a pressure between 1 and 4 MPa. Relief valves have been installed in the liquid feed lines to protect the pump and, in the case of blockage, to eliminate pressure buildup in the feed lines. Temperature control (in the range between 15 and 100 °C) is performed by flowing, in the reactor jacket, water at 15 °C or steam at 150 °C as cooling and heating fluid, respectively. The maximum cooling capacity is 4600 J/s. The reactor is equipped with an electronic PD temperature controller and a pressure transducer capable of detecting a pressure change of 7 KPa. The monomer feed flow rate is monitored on-line through a flow meter. It is worth noting that since the reaction is carried out at constant pressure and the monomer solubility in the reacting system is negligible, the monomer feed flow rate is substantially equal to the reaction rate. Thus, the flow meter provides the on-line monitoring of the conversion. A scheme of the pilot plant reactor is shown in Figure 1.

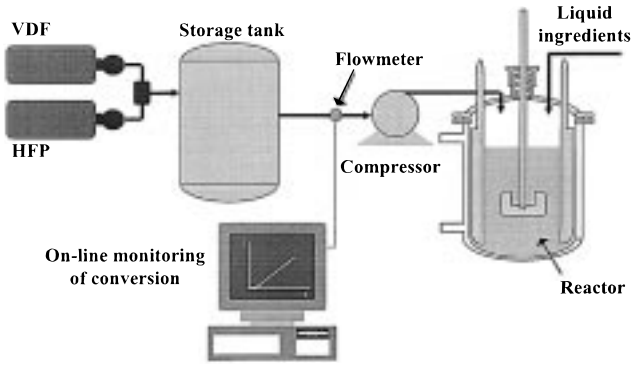

Figure 1. Scheme of the pilot plant.

1.3. Polymer Characterization. The characterization of the polymer chains is designed so as to give information about the types of reactions involved in the polymerization process and their kinetics. This is based on the measurement of the chain length and end group distributions.

The MWD of the VDF−HFP copolymer has been measured through gel permeation chromatography (GPC). The analyses were performed in tetrahydrofuran at 30 °C using a set of four ultrastyragel styrene-divinylbenzene columns of porosity 10^3, 10^4, 10^5, and 10^6, respectively, equipped with a detector based on the refractive index measurement.

Since, as discussed later, under the experimental polymerization conditions adopted in this work, the VDF−HFP copolymer is only slightly branched, the MWD can be estimated directly from GPC measurements, neglecting the effect of long-chain branching. This has been verified following the algorithm proposed by Ram and Miltz,[1] where the relationship between the intrinsic viscosity and the molecular weight is approximated with a polynomial expression. Additional information relative to the entire polymer sample (the intrinsic viscosity) has been used to evaluate through an iterative procedure the value of the adjustable parameters of the polynomial equation.

The type and number of polymer chain ends have been measured by NMR (300 MHz).[2] The polymer samples were dissolved in acetone-d_6, and ^{1}H NMR spectra were used to determine the concentration of chain end groups per mole of polymer. The average number of chain ends per macromolecule is calculated by dividing the chain end concentration value by the average number molecular weight, given by GPC. The overall number of the average chain ends per macromolecule, decreased by two, provides the average number of branches per macromolecule.

2. Modeling Emulsion Copolymerization of VDF and HFP

In the following the kinetic model of the emulsion copolymerization of VDF and HFP in a semi-batch reactor is presented. According to the pseudokinetic approach,[3,4] the evolution of the system is described in terms of an equivalent homopolymer whose kinetic constants are suitable averages of the true copolymerization kinetic parameters. In this way, the numerical effort for solving the model reduces to that typical of homopolymerization reactions.

The model is developed using the following main assumptions, which are well-suited for the system under examination.

(1) Negligible Mass-Transport Limitations: The interphase partitioning of monomers and CTA is at equilibrium conditions at any time during polymerization.

(2) QSSA, LCA, and Ultimate Model: Quasi-steady-state assumption (QSSA) is considered for the radical species. Moreover, because the large molecular weights usually obtained, the long-chain assumption (LCA) is introduced, thus neglecting any dependence of chain composition upon length. Finally, the copolymerization kinetics has been described using the ultimate model, thus assuming that the reactivity of an active chain is determined only by the last added monomer unit.

(3) Pseudobulk System: From independent measurements, which are discussed elsewhere,[5] it has been found that the rate of polymerization is independent of the particle number. Therefore, this is a noncompartimentalized system, where the number of radicals per particle is sufficiently large to behave like a bulk polymerization. In addition, with respect to standard applications, the particle size distribution is not a relevant polymer quality parameter. Therefore, the nucleation process is not modeled and the particle number is not computed. This is coherent with a pseudobulk system where the relevant quality is only the overall radical concentration, Y_0, as opposed to a segregated system where both the number of polymer particles and the number of radicals per particle play an important role on the polymerization kinetics.

(4) Homogeneous Particle: Because of the very limited crystallinity of the copolymer VDF−HFP, it is expected that the reactants are homogeneously distributed inside the polymer particles.

(5) Negligible Water Solubility: This is due to the strongly hydrophobic nature of the monomers.

2.1. Kinetic Scheme. The detailed kinetic scheme of VDF−HFP copolymerization involves several chemical reactions. One complication arises from the fact that in the free-radical VDF−HFP copolymerization, three different radical species can be formed as a result of the following propagation reactions:

HFP addition

$$R^{\bullet} + CF_2 = CF(CF_3) \rightarrow RCF_2CF(CF_3)^{\bullet}$$

VDF head−tail addition

$$R^{\bullet} + CF_2 = CH_2 \rightarrow RCH_2CF_2^{\bullet}$$

VDF head−head addition

$$R^{\bullet} + CF_2 = CH_2 \rightarrow RCF_2CH_2^{\bullet}$$

It should be noted that the head−head VDF addition reaction, resulting in a $CH_2^{\bullet}$ radical type, takes place in 4−7% of the VDF addition events, depending upon the reaction temperature. Since each of the three radicals above can, in principle, undergo all the various reactions typical of free-radical polymerizations, it is clear that the resulting kinetic scheme tends to be rather large. To determine the most important reactions present in the system, a detailed characterization analysis has been performed based on NMR. By identifying the most important chain end types and, based on mechanistic considerations, eliminating less favored reactions, the simplified kinetic scheme shown in Figure 2 has been derived. We do not describe here the derivation of this scheme, but only discuss briefly its main features, and then proceed to its validation by comparison with the various obtained experimental data.

Initiation reaction

$$SO_4^{\bullet -} + CH_2 = CF_2 \xrightarrow{k_I} {}^{\bullet}CF_2\mathbf{CH_2OH}$$

Chain transfer to monomer

$$RCH_2CF_2^{\bullet} + CH_2 = CF_2 \xrightarrow{k_{fm\,11}} {}^{\bullet}CF_2CH_3 + R\mathbf{CH} = \mathbf{CF_2}$$

Chain transfer to Ethyl Acetate

$$RCH_2CF_2^{\bullet} + CH_3COOCH_2CH_3 \xrightarrow{k_{ft_1}} \mathbf{CH_3COO\overset{\bullet}{C}HCH_3} + RCH_2\mathbf{CF_2H}$$

Chain transfer to polymer

$$RCH_2CF_2^{\bullet} + RCH_2R \xrightarrow{k_{fp_{11}}} RCH_2\mathbf{CF_2H} + R\overset{\bullet}{C}HR$$

Propagation to TDB reaction

$$R^{\bullet} + R\mathbf{CH} = \mathbf{CF_2} \xrightarrow{K_p^*} R\overset{\bullet}{C}HR$$

Bimolecular termination by disproportionation

$$RCH_2CF_2^{\bullet} + RCH_2CF_2^{\bullet} \xrightarrow{k_{td\,11}} R\mathbf{CH} = \mathbf{CF_2} + RCH_2\mathbf{CF_2H}$$

Backbiting reaction

$$RCH_2CF_2CH_2CF_2^{\bullet} \xrightarrow{k_{bb1}} R\overset{\bullet}{C}HCF_2CH_2\mathbf{CF_2H}$$

$$RCH_2CF_2CF_2CH_2^{\bullet} \xrightarrow{k_{bb2}} R\overset{\bullet}{C}HCF_2CF_2\mathbf{CH_3}$$

Figure 2. Reaction scheme for the VDF−HFP copolymerization. The produced polymer chain end groups are in bold.

The chemistry of this copolymerization is characterized by the mobility of the hydrogen atoms of VDF. This is responsible for the chain transfer to monomer and to polymer reactions as well as for the bimolecular termination by disproportionation. Note that all these reactions involve the $CF_2^{\bullet}$-type radical, which then appears as the dominant one in this system. An exception to this general behavior is given by the last two reactions in Figure 2, representing an intramolecular chain transfer to a polymer (so-called backbiting) reaction. In this case, also the $CH_2^{\bullet}$-type is involved. It is worth noting that the backbiting reaction produces a short-chain branch, which can be neglected when modeling the MWD, while it has to be accounted for when considering the chain end distribution.

Let us now go back to the three reactions characterized by the high mobility of the hydrogens in VDF. Chain transfer to monomer and bimolecular termination by disproportionation involve the abstraction of hydrogen from the β-carbon of the reacting radical. The radical becomes a dead polymer chain with a terminal double bond (TDB), while the hydrogen is captured by another active chain in the case of disproportionation, or by a monomer unit in the case of chain transfer to a monomer reaction. Subsequently, during the polymerization reaction, the formed TDB can propagate with a growing radical through the usual propagation mechanism. The resulting chain is the combination of these two chains with an additional trifunctional unit (i.e., with a long-chain branch).

Initiation

$$I \xrightarrow{k_I} 2R(1,0)$$

Propagation

$$R(j,n) + M \xrightarrow{K_p} R(j+1,n) \qquad K_p = \sum_{i,s} k_{p_{is}} \varphi_i f_s$$

Chain transfer to monomer

$$R(j,n) + M \xrightarrow{K_{fm}} P(j,n) + R(1,0) \qquad K_{fm} = \sum_{i,s} k_{fm_{is}} \varphi_i f_s$$

Chain transfer to a CTA

$$R(j,n) + \Gamma \xrightarrow{K_{ft}} P(j,n) + R(1,0) \qquad K_{ft} = \sum_{i} k_{ft_i} \varphi_i$$

Chain transfer to polymer

$$R(j,n) + P(r,k) \xrightarrow{K_{fp}} P(j,n) + R(r,k+1) \qquad K_{fp} = \sum_{i,s} k_{fp_{is}} \varphi_i Y_s$$

Propagation to TDB

$$R(j,n) + P(r,k) \xrightarrow{K_p^*} R(j+r,n+k+1) \qquad K_p^* = \sum_{i} k_{p_i}^* \varphi_i$$

Bimolecular termination by disproportionation

$$R(j,n) + R(r,k) \xrightarrow{K_{td}} P(j,n) + P(r,k) \qquad K_{td} = \sum_{i,s} k_{td_{is}} \varphi_i \varphi_s$$

Figure 3. Kinetic scheme of VDF−HFP copolymerization together with the definition of the relevant pseudokinetic rate constant, K_n.

On the other hand, in the case of a chain transfer to polymer reaction, a hydrogen in the backbone of the polymer chain is abstracted by a growing radical which terminates. Then, the radical in the backbone of the chain grows, leading to a new long-chain branch. It is clear that long-chain branches have to be accounted for when modeling the MWD as well as the chain end distribution.

From the chemical reactions in Figure 2, the kinetic scheme for calculating the MWD in VDF−HFP copolymerization is readily obtained as shown in Figure 3. $R(j,n)$ and $P(j,n)$ indicate the concentrations of active and terminated polymer chains with j monomer units and n long-chain branches, respectively. In the same figure, the expressions for the relevant pseudokinetic rate constants are also reported, where $f_i = M_i/\sum_s M_s$, and Y_s indicates the cumulative copolymer composition.

2.2. Macroscopic Monomer Balance Equations. The mass-balance equation for the generic ith monomer in a system of NM monomeric species in a semibatch reactor is given by

$$\frac{dM_i^T}{dt} = \bar{Q} w_i - K_{p_i} M_i Y_0 \frac{V_w}{V_p} \qquad (i = 1, ..., NM) \qquad (1)$$

where M_i^T represents the overall ith monomer concentration, M_i is the monomer concentration in the polymer particles, Y_0 is the radical concentration in the polymer particles, K_{p_i} is the pseudopropagation rate constant, V_p is the total volume of polymer particles, V_w is the water volume in the reactor, $\bar{Q}$ is the feed flow rate specific to the unit volume of water, and w_i is the ith monomer molar fraction in the feed.

For the overall amount of produced polymer (M_c) we have

$$\frac{dM_c}{dt} = \sum_{j=1}^{NM} K_{p_j} M_j Y_0 \frac{V_w}{V_p} \qquad (2)$$

In the above equations, all concentrations are conventionally specific to the unit volume of the water phase, which is the only phase inside the reactor whose volume remains constant during the reaction.

According to the pseudohomopolymerization approach,[3,4] the pseudopropagation rate constant is given by

$$K_{p_i} = \sum_{j=1}^{NM} k_{p_{ji}} \varphi_j \qquad (i = 1, ..., NM) \qquad (3)$$

where $k_{p_{ji}}$ are the *true* propagation rate constants of the copolymer and φ_j is the probability of having an active chain with monomer j as terminal. The probability φ_j can be calculated from the monomer instantaneous concentrations in the polymer particles and the crosspropagation rate constants, $k_{p_{ji}}$ as follows:

$$\varphi_1 = \frac{k_{p_{21}} M_1}{k_{p_{21}} M_1 + k_{p_{12}} M_2}; \qquad \varphi_2 = 1 - \varphi_1 \qquad (4)$$

By dividing eq 1 by eq 2, a monomer balance is obtained where the independent variable is the mass of produced polymer M_c instead of time:

$$\frac{dM_i^T}{dM_c} = Q w_i - \frac{K_{p_i} M_i}{\sum_j K_{p_j} M_j} = Q w_i - \bar{Y}_i \qquad (i = 1, ..., NM) \qquad (5)$$

where Q is the overall monomer's feed flow rate specific to the amount of produced polymer (i.e., grams of monomer mixture fed per gram of produced polymer) and $\bar{Y}_i$ is the copolymer instantaneous composition. This is defined as the ratio between the rate of consumption of each monomer, $K_{p_i} M_i$, and the total rate of polymer production:

$$\bar{Y}_i = \frac{K_{p_i} M_i}{\sum_j K_{p_j} M_j} \qquad (i = 1, ..., NM) \qquad (6)$$

Note that the only parameters involved in the equation above are the monomer concentrations in the reaction locus and the ratios between the average propagation rate constants. In the case of binary systems, using eqs 3 and 4, eq 6 for component 1 reduces to the following well-known equation for the instantaneous copolymer composition:[6]

$$\bar{Y}_1 = \frac{r_1 (M_1/M_2) + 1}{(1 + r_1)(M_1/M_2) + 1 + r_2} \qquad \bar{Y}_2 = 1 - \bar{Y}_1 \qquad (7)$$

where r_1 and r_2 are the reactivity ratios.

By solving the system of equations in (5), the evolution of the polymer composition as a function of conversion is obtained. Note that the active chains concentration Y_0 is not required. This is a consequence of using

conversion (or polymer amount) as the independent variable instead of time.

About monomer partitioning among the phases present in the system (i.e., gaseous, aqueous, and polymer), the following relations have been used. The monomer concentration in the gaseous phase, M_i^g, is calculated through the following equation:

$$M_i^g = \frac{P y_i V_g}{ZRTV_w} \qquad (i = 1, ..., NM) \tag{8}$$

where P indicates the reactor pressure, y_i the monomer molar fraction in the gas phase, V_g the volume of the gas phase, Z the compressibility factor, R the gas constant, and T the reactor temperature. In this work, the Z value has been estimated using the Peng−Robinson equation of state.[7] The partitioning of the monomers between gaseous phase and polymer particles is described using Henry's law, which, with the adopted notation, becomes

$$M_i = \frac{h_i \mathrm{MW}_c}{\rho_c} M_c P y_i \qquad (i = 1, ..., NM) \tag{9}$$

where h_i is the ith monomer Henry's constant, ρ_c is the polymer density, and MW_c is the molecular weight of the average monomer unit in the copolymer chain. This is a function of the copolymer composition through the following equation:

$$\mathrm{MW}_c = \int_0^{M_c} \sum_i \mathrm{MW}_i \bar{Y}_i \frac{\mathrm{d}M_c'}{M_c} \tag{10}$$

where MW_i indicates the molecular weight of the ith monomer. However, under conditions of negligible compositional drift (as in the case under examination here), this value is practically constant during the polymerization process. As mentioned above, the monomer concentration in the aqueous phase is neglected.

The mass-balance equations for the initiator concentration in the water phase, I, and the concentration of the chain-transfer agent in the polymer particles, Γ, are respectively

$$\frac{\mathrm{d}I}{\mathrm{d}M_c} = -\frac{k_I}{K_p} \frac{I}{MY_0} \frac{V_p}{V_w} \tag{11}$$

$$\frac{\mathrm{d}\Gamma}{\mathrm{d}M_c} = -C_{ft} \frac{\Gamma}{M} \tag{12}$$

where C_{ft} is the ratio between the pseudokinetic rate constant of chain transfer to the chain-transfer agent and the pseudopropagation constant, K_p.

Finally, the initiator is considered completely water-soluble, while the chain-transfer agent concentration in the polymer particles is calculated assuming a linear partitioning between aqueous solution and polymer particles:

$$\Gamma = \gamma \Gamma^w \frac{V_p}{V_w} \tag{13}$$

where γ is the partitioning coefficient and Γ^w is the CTA concentration in the aqueous phase.

2.3. Evolution of the Molecular Weight Distribution. A critical examination of the kinetic scheme in Figure 3 shows that the VDF−HFP copolymerization may lead, depending upon the polymerization conditions, to polymer gelation. This is due to the simultaneous occurrence of chain transfer to polymer and a chain combination reaction, such as bimolecular termination by combination or propagation to TDB, which is a sufficient condition to produce an infinite polymer network, usually indicated as a gel.[8,9] This theoretical expectation is confirmed by experimental evidences of gelation in VDF−HFP copolymerization reported in the literature.[10,11] Indeed, the presence of branched chains and possibly a gel phase causes significant problems in computing the MWD.

In the case of linear polymer chains, several models for the prediction of MWD, both in homogeneous and heterogeneous polymerization processes, are available (cf., for example, refs 12−17). They are based on different approaches and use different solution strategies but provide substantially equivalent results. Among the various alternatives, a convenient choice is to use the kinetic approach to derive the population balance equations, which constitute the model, and the method of moments to solve them. The main advantage of this approach is the limited computational effort, being the original set of infinite equations lumped into a set of few moment equations.[18] From the first few leading moments of the unknown distribution, significant averages of the molecular weight are readily obtained and, at least in the simpler cases, the entire distribution can be reconstructed.[19]

The situation is more complicated for branched polymers. Also in this case, after the pioneering works by Flory[20] and Stockmayer,[21,22] appropriate models have been developed both for homogeneous[23−25] and heterogeneous reactions.[26] Using the kinetic approach and solving through the method of moments, numerical difficulties usually arise because of the broadness of the MWD. In the case of gel formation, these difficulties become even more evident as indicated by the divergence of the moments of order larger than 1. An elegant solution of this problem is the recently proposed numerical fractionation.[27] The basic idea is to fractionate the original broad MWD into several, narrower subdistributions, each of which can be approximated in terms of only a few moments. This allows one to account for wider MWDs as well as to simulate the gel formation.[26,27] This numerical technique, which has been used both in homogeneous[27] and heterogeneous[28,29] systems, has been shown to drastically improve the accuracy of the classical method of moments, although it also has limitations, which become significant for very wide MWDs.

Its application to the system under consideration is presented in the following, where we briefly discuss first the classical moment equations and then their numerically fractionated approximation.

2.3.1. Overall Moment Equations. With reference to the kinetic scheme in Figure 3, the population balance equations of active, R_j, and terminated chains, P_j, having j monomeric units and any number of branches can be written as follows:

$$\frac{dP_j}{dt} = (K_{fm}MR_j + K_{ft}\Gamma R_j + K_{fp}R_j\sum_k kP_k + -K_{fp}jP_j\sum_k R_k - K_p^*\alpha P_j\sum_k R_k + K_{td}R_j\sum_k R_k)\frac{V_w}{V_p} \quad (14)$$

$$\frac{dR_j}{dt} = (\delta_j R_d + \delta_j K_{fm}M\sum_k R_k + \delta_j K_{ft}\Gamma\sum_k R_k + K_pMR_{j-1} - K_pMR_j - K_{fm}MR_j - K_{ft}\Gamma R_j + K_{fp}jP_j\sum_k R_k - K_{fp}R_j\sum_k kP_k - K_p^*\alpha R_j\sum_k P_k + K_p^*\alpha\sum_{k=1}^{j} R_{j-k}P_k - K_{td}R_j\sum_k R_k)\frac{V_w}{V_p} \quad (15)$$

In the above equations, R_d is the rate of initiation, $\delta_j = 1$ for $j = 1$ and $\delta_j = 0$ for $j > 1$ is the Kronecher δ, M and Γ are the concentrations in the polymer particles of the monomer and CTA, respectively, and α is the fraction of polymeric chains having a TDB.

According to the method of moments, the equations of the first three leading moments of the MWD of the terminated chains, Q_i, can be derived either directly from the moment definition or through the generating functions method.[30] Using polymer conversion as the independent variable, which means to divide eq 14 by the overall rate of polymer production specific to the unit volume of water, $K_pMY_0V_w/V_p$, the following equations for the moments are obtained:

$$\frac{dQ_0}{dM_c} = C_{fm} + C_{ft}\frac{\Gamma}{M} - C_p^*\alpha\frac{Q_0}{M} + C_{td}\frac{Y_0}{M} \quad (16)$$

$$\frac{dQ_1}{dM_c} = 1 + \bar{R}_d + C_{fm} + C_{ft}\frac{\Gamma}{M} \quad (17)$$

$$\frac{dQ_2}{dM_c} = 2\left(1 + C_p^*\alpha\frac{Q_1}{M}\right)\times \frac{1 + \bar{R}_d + C_{fm} + C_{ft}\frac{\Gamma}{M} + C_{fp}\frac{Q_2}{M} + C_p^*\alpha\frac{Q_1}{M}}{C_{fm} + C_{ft}\frac{\Gamma}{M} + C_{fp}\frac{Q_1}{M} + C_{td}\frac{Y_0}{M}} + 1 + \bar{R}_d + C_{fm} + C_{ft}\frac{\Gamma}{M} \quad (18)$$

where Y_0 indicates the 0th-order moment of the active chains distribution (i.e., the concentration of active chains of any type in the polymer particles), $\bar{R}_d$ is defined as $R_dV_p/K_pMY_0V_w$, and the C_n parameters are the ratios between the pseudokinetic rate constant of the nth kinetic event in Figure 3 and the pseudopropagation rate constant K_p.

2.3.2. Fractionated Moment Equations. According to the numerical fractionation technique,[27] the overall polymer population is divided into several fractions (generations), each one characterized by a "narrower" distribution. The rules on which this fractionation is based arise from the kinetic scheme. By inspection of Figure 3, it is apparent that two different modes of chain growth exist. The first one is the classical chain propagation. The second is the propagation to the TDB reaction which results in a step growth of the polymer chain, since it links two macromolecules into a single one. As a consequence, the resulting polymer chain has properties (such as size and number of long-chain branches) significantly different from those of the two original macromolecules. This is the event that we regard as responsible for a generation change. Accordingly, we derive the following fractionation rules: when a polymer chain of the ith generation undergoes a propagation to the TDB reaction with a macromolecule belonging to the same generation, the resulting macromolecule belongs to the $(i + 1)$ generation. All other reactions in the scheme under examination do not imply a generation change. So, for example, the propagation to TDB involving a macromolecule of the ith generation and one of a lower generation produces a molecule which still belongs to the ith generation. The only exception to this general rule is the movement from the 0th generation (by definition constituted of the linear chains) to the first generation which is caused also by transfer to the polymer.

Because of the selected rules for generation transition, it is expected that the average size of the macromolecules inside each generation increases with the generation order and that the chains within a single generation are more uniform than those in the entire distribution. We now apply the method of moments to each generation, thus leading to a set of moment equations for each of them. Because of this uniformity among the macromolecules within each generation, the first three moments are expected to be sufficient to reconstruct the MWD of the generation with reasonable accuracy. The MWD of the overall polymer population is then obtained by summing up the MWDs of each generation.

Using the fractionation rules indicated above, the population balances of growing and terminated polymer chains within each generation can be derived. In particular, for the terminated polymer chains having j monomeric units and belonging to the nth generation, P_j^n, the following balances apply:

$$\frac{dP_j^n}{dt} = (K_{fm}MR_j^n + K_{ft}\Gamma R_j^n + K_{fp}R_j^n\sum_k kP_k + -K_{fp}jP_j^n\sum_k R_k - K_p^*\alpha P_j^n\sum_k R_k + K_{td}R_j\sum_k R_k)\frac{V_w}{V_p} \quad (19)$$

In the case of active chains, R_j^n indicates the concentration of chains having j monomeric units and belonging to the nth generation. The following balance equations are obtained, where the first two generations have been considered explicitly because of the presence of some characteristic terms:

$$\frac{dR_j^0}{dt} = (\delta_j R_d + K_pMR_{j-1}^0 - K_pMR_j^0 - K_{fm}MR_j^0 + -K_{ft}\Gamma R_j^0 - K_{fp}R_j^0\sum_k kP_k - K_p^*\alpha R_j^0\sum_k P_k + -K_{td}R_j^0\sum_k R_k)\frac{V_w}{V_p} \quad (20)$$

$$\frac{dR_j^1}{dt} = (K_p M R_{j-1}^1 - K_p M R_j^1 - K_{fm} M R_j^1 - K_{ft} \Gamma R_j^1 + -K_{fp} R_j^1 \sum_k k P_k + K_{fp} j (P_j^0 + P_j^1) \sum_k R_k - K_p^* \alpha R_j^1 \sum_k P_k + K_p^* \alpha \sum_{k=1}^{j-1} (R_{j-k}^0 P_k^0 + R_{j-k}^0 P_k^1 + R_{j-k}^1 P_k^0) - K_{td} R_j^1 \sum_k R_k) \frac{V_w}{V_p} \quad (21)$$

$$\frac{dR_j^n}{dt} = (K_p M R_{j-1}^n - K_p M R_j^n - K_{fm} M R_j^n - K_{ft} \Gamma R_j^n + -K_{fp} R_j^n \sum_k k P_k + K_{fp} j P_j^n \sum_k R_k - K_p^* \alpha R_j^n \sum_k P_k + K_p^* \alpha \sum_{h=0}^{n-1} \sum_{k=1}^{j-1} (R_{j-k}^{n-1} P_k^{n-1} + R_{j-k}^n P_k^h + R_{j-k}^h P_k^n) - K_{td} R_j^n \sum_k R_k) \frac{V_w}{V_p} \qquad (n \geq 2) \quad (22)$$

When using the method of moments, the following equations for the kth order moment of the MWD of the terminated polymer belonging to the nth generation, μ_k^n is obtained:

$$\frac{d\mu_k^n}{dM_c} = \left(C_{fm} + C_{ft}\frac{\Gamma}{M} + C_{fp}\frac{Q_1}{M} + C_{td}\frac{Y_0}{M}\right)\frac{\lambda_k^n}{Y_0} - C_{fp}\frac{\mu_{k+1}^n}{M} + -C_p^* \alpha \frac{\mu_k^n}{M} \quad (23)$$

where again conversion rather than time has been used as the independent variable. From the above equation, it is apparent that the evaluation of μ_k^n requires the knowledge of μ_{k+1}^n, which means that a closure equation is necessary. This can be readily obtained using the same model distribution that we intend to use to reconstruct the MWD from its moments.[31] In this work we have used a Gamma distribution as model distribution and the first three moments to reconstruct the MWD of each generation. Thus, we used the following closure equation for the third-order moment:[31]

$$\mu_3^n = 2\frac{(\mu_2^n)^2}{\mu_1^n} - \frac{\mu_2^n \mu_1^n}{\mu_0^n} \quad (24)$$

Note that the closure problem does not affect the calculation of the first three moments of the overall MWD of the terminated chains given by eqs 16−18. These are obtained by summing up eqs 23 (for $k = 0$, 1, 2) with n going from 0 to ∞ and combining the resulting equations with those obtained by summation of the corresponding equations for the active polymer to be described in the following. In this process the terms involving higher order moments cancel out.

The kth order moments, λ_k^n, of the active chain distribution of the nth generation are obtained from eq 20−22. In particular, the resulting expressions for the first three moments of the MWD of the polymer belonging to each generation are reported in the following. Three sets of moment equations are reported, for $n = 0$, 1 and $n \geq 2$, respectively.

$$\frac{d\lambda_0^0}{dM_c} = \bar{R}_d + C_{fm} + C_{ft}\frac{\Gamma}{M} + -\left(C_{fm} + C_{ft}\frac{\Gamma}{M} + C_{fp}\frac{Q_1}{M} + C_p^*\alpha\frac{Q_0}{M} + C_{td}\frac{Y_0}{M}\right)\frac{\lambda_0^0}{Y_0} \quad (25)$$

$$\frac{d\lambda_1^0}{dM_c} = \bar{R}_d + C_{fm} + C_{ft}\frac{\Gamma}{M} + \frac{\lambda_0^0}{Y_0} + -\left(C_{fm} + C_{ft}\frac{\Gamma}{M} + C_{fp}\frac{Q_1}{M} + C_p^*\alpha\frac{Q_0}{M} + C_{td}\frac{Y_0}{M}\right)\frac{\lambda_1^0}{Y_0} \quad (26)$$

$$\frac{d\lambda_2^0}{dM_c} = \bar{R}_d + C_{fm} + C_{ft}\frac{\Gamma}{M} + \frac{\lambda_0^0}{Y_0} + 2\frac{\lambda_1^0}{Y_0} + -\left(C_{fm} + C_{ft}\frac{\Gamma}{M} + C_{fp}\frac{Q_1}{M} C_p^*\alpha\frac{Q_0}{M} + C_{td}\frac{Y_0}{M}\right)\frac{\lambda_2^0}{Y_0} \quad (27)$$

$$\frac{d\lambda_0^1}{dM_c} = -\left(C_{fm} + C_{ft}\frac{\Gamma}{M} + C_{fp}\frac{Q_1}{M} + C_p^*\alpha\frac{Q_0}{M} + C_{td}\frac{Y_0}{M}\right) \times \frac{\lambda_0^1}{Y_0} + C_{fp}\frac{\mu_0^1 + \mu_1^1}{M} + C_p^*\alpha\frac{\mu_0^0\lambda_0^0 + \mu_0^1\lambda_0^0 + \mu_0^0\lambda_0^1}{M} \quad (28)$$

$$\frac{d\lambda_1^1}{dM_c} = \frac{\lambda_0^1}{Y_0} - \left(C_{fm} + C_{ft}\frac{\Gamma}{M} + C_{fp}\frac{Q_1}{M} + C_p^*\alpha\frac{Q_0}{M} + C_{td}\frac{Y_0}{M}\right) \times \frac{\lambda_1^1}{Y_0} + C_{fp}\frac{\mu_2^0 + \mu_2^1}{M} + C_p^*\alpha\frac{\mu_1^0\lambda_0^0 + \mu_0^0\lambda_1^0 + \mu_1^1\lambda_0^0 + \mu_0^1\lambda_1^0 + \mu_1^0\lambda_0^1 + \mu_0^0\lambda_1^1}{M} \quad (29)$$

$$\frac{d\lambda_2^1}{dM_c} = \frac{2\lambda_1^1 + \lambda_0^1}{Y_0} + C_{fp}\frac{\mu_3^0 + \mu_3^1}{M} - \left(C_{fm} + C_{ft}\frac{\Gamma}{M} + C_{fp}\frac{Q_1}{M} + C_p^*\alpha\frac{Q_0}{M} + C_{td}\frac{Y_0}{M}\right)\frac{\lambda_2^1}{Y_0} + C_p^*\alpha[(\mu_2^0\lambda_0^0 + 2\mu_1^0\lambda_1^0 + \mu_0^0\lambda_2^0 + \mu_2^1\lambda_0^0 + 2\mu_1^1\lambda_1^0 + \mu_0^1\lambda_2^0 + \mu_2^0\lambda_0^1 + 2\mu_1^0\lambda_1^1 + \mu_0^0\lambda_2^1)/M] \quad (30)$$

$$\frac{d\lambda_0^n}{dM_c} = -\left(C_{fm} + C_{ft}\frac{\Gamma}{M} + C_{fp}\frac{Q_1}{M} + C_p^*\alpha\frac{Q_0}{M} + C_{td}\frac{Y_0}{M}\right)\frac{\lambda_0^n}{Y_0} + C_{fp}\frac{\mu_1^n}{M} + C_p^*\alpha\sum_{i=0}^{n-1}\frac{\mu_0^{n-1}\lambda_0^{n-1} + \mu_0^i\lambda_0^n + \mu_0^n\lambda_0^i}{M} \quad (31)$$

$$\frac{d\lambda_1^n}{dM_c} = \frac{\lambda_0^n}{Y_0} - \left(C_{fm} + C_{ft}\frac{\Gamma}{M} + C_{fp}\frac{Q_1}{M} + C_p^*\alpha\frac{Q_0}{M} + C_{td}\frac{Y_0}{M}\right) \times \frac{\lambda_1^n}{Y_0} + C_{fp}\frac{\mu_2^n}{M} + C_p^*\alpha\sum_{i=0}^{n-1}[(\mu_1^{n-1}\lambda_0^{n-1} + \mu_0^{n-1}\lambda_1^{n-1} + \mu_1^i\lambda_0^n + \mu_0^i\lambda_1^n + \mu_1^n\lambda_0^i + \mu_0^n\lambda_1^i)/M] \quad (32)$$

$$\frac{d\lambda_2^n}{dM_c} = \frac{2\lambda_1^n + \lambda_0^n}{Y_0} + C_{fp}\frac{\mu_3^n}{M} - \left(C_{fm} + C_{ft}\frac{\Gamma}{M} + C_{fp}\frac{Q_1}{M} + C_p^*\alpha\frac{Q_0}{M} + C_{td}\frac{Y_0}{M}\right)\frac{\lambda_2^n}{Y_0} + C_p^*\alpha\sum_{i=0}^{n-1}[(\mu_2^{n-1}\lambda_0^{n-1} + 2\mu_1^{n-1}\lambda_1^{n-1} + \mu_0^{n-1}\lambda_2^{n-1} + \mu_2^i\lambda_0^n + 2\mu_1^i\lambda_1^n + \mu_0^i\lambda_2^n + \mu_2^n\lambda_0^i + 2\mu_1^n\lambda_1^i + \mu_0^n\lambda_2^i)/M] \quad (33)$$

When applying the quasi-steady-state approximation (QSSA) to eq 25−33, the system of differential equations reduces to an algebraic system of equations, which can

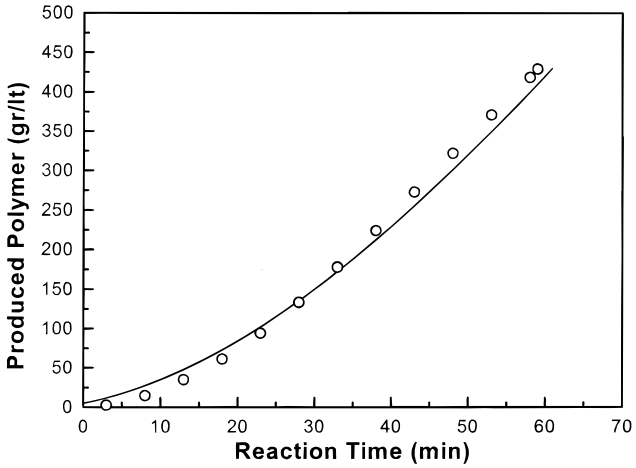

Figure 4. Polymer produced as a function of time for runs 1−3. Solid line: model prediction. Circles: experimental data.

be solved analytically. Thus, the values of λ_k^n appearing in eq 23 become available and the three leading moments of the MWD are readily calculated for each generation by integrating eq 23 as a function of the polymer produced. Finally, the *k*th order moments of the overall MWD are obtained by summing up the corresponding *k*th order moments of each generation.

2.4. Evaluation of the Chain End Groups Distribution. From the polymerization scheme shown in Figure 2, we can identify the polymer chain end groups produced during the polymerization reaction.

The thermal decomposition of APS in aqueous solutions leads to the formation of CH_2OH chain end groups, eventually resulting from the complete hydrolysis of the sulfate intermediates.[11] The sulfate end groups, $CF_2OSO_3^-$, were in fact not found on the polymer.[2] Under typical reaction conditions, CF_2H is the most common chain end group. It is formed by several reactions, including chain transfer to polymer, chain transfer to ethyl acetate, termination by disproportionation, and backbiting reactions, which all have in

Table 2. Physicochemical Parameters of the Model

parameter	numerical value	source (ref no.)
reactivity ratios:		
$R_{VDF-HFP}$	5	11
$R_{HFP-VDF}$	0	11

parameter	VDF	HFP	source (ref no.)
Henry constant (kmol/Pa·m^3)	3.1×10^{-7}	4.8×10^{-7}	32
critical temp (K)	303.0	358.6	32
critical pressure (MPa)	4.37	3.20	32
acentric factor	0.17303	0.35796	32

Peng−Robinson Equation of State: Mixing Rules (ref no. 7)

$$a = \sum_i \sum_j (a_i a_j)^{1/2} y_i y_j \qquad b = \sum_i b_i y_i$$

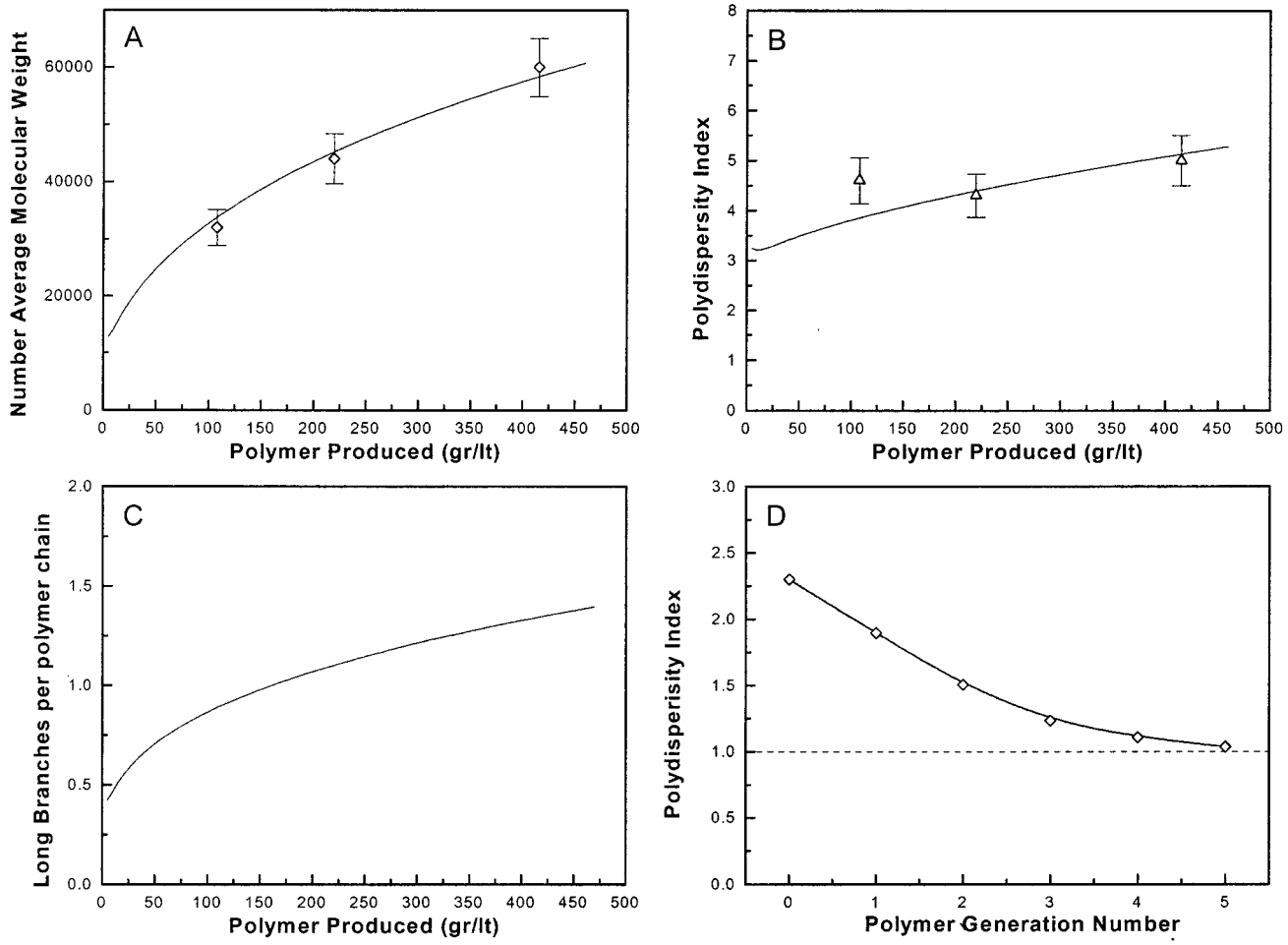

Figure 5. VDF−HFP copolymerization (runs 1−3). (A) Number-average molecular weight as a function of the polymer produced. Solid line: model prediction. Diamond: experimental data from GPC measurements. (B) Polydispersity index as a function of the polymer produced. Solid line: model prediction. Triangles: experimental data from GPC measurements. (C) Calculated long-chain branches per macromolecule as a function of the polymer produced. (D) Calculated polydispersity index of the MWD of each polymer generation.

Table 3. Estimated Values of the Kinetic Parameters of the Model

kinetic parameter		numerical value
K_p	$m^3/kmol \cdot s$	2.1×10^3
C_{fm}		6.5×10^{-4}
C_{ft}		1.1×10^{-2}
C_{fp}		2.8×10^{-5}
C_p^*		9.3×10^{-3}
C_{td}		25.7
C_{bb}	$kmol/m^3$	1.3×10^{-3}
γ		4.0
β		0.85

common the abstraction of a hydrogen by the $CF_2^\bullet$ radical. The CH_3 chain end group is formed by chain transfer to monomer and backbiting reactions. In addition to the CF_2H group, the chain transfer to ethyl acetate reaction produces another chain end, that is, the fragment of ethyl acetate $CH_3COOCH(CH_3)$. Finally, as discussed earlier, the TDB is formed by chain transfer to monomer and termination by disproportionation reactions. It is worth recalling that this is the only reactive chain end group, as it can be consumed by the propagation to TDB reaction.

The concentration of the chain end groups can be calculated through the following balances:

$$\frac{d(CH_2OH)}{dM_c} = 2\frac{k_I}{K_p}\frac{I}{MY_0}\frac{V_p}{V_w} \quad (34)$$

$$\frac{d(CF_2H)}{dM_c} = C_{ft}\frac{\Gamma}{M} + \frac{1}{2}C_{td}\frac{Y_0}{M} + C_{fp}\frac{Q_1}{M} + C_{bb}\beta\frac{1}{M}\frac{V_p}{V_w} \quad (35)$$

$$\frac{d(CH_3)}{dM_c} = C_{fm} + C_{ft}\frac{\Gamma}{M} + C_{bb}(1-\beta)\frac{1}{M}\frac{V_p}{V_w} \quad (36)$$

$$\frac{d(CH_3COOCH(CH_3))}{dM_c} = C_{ft}\frac{\Gamma}{M} \quad (37)$$

$$\frac{d(TDB)}{dM_c} = C_{fm} + \frac{1}{2}C_{td}\frac{Y_0}{M} - C_p^*\alpha\frac{Q_0}{M} \quad (38)$$

where I is the initiator concentration and β represents the fraction of backbiting reactions which lead to the CF_2H end group (i.e., $\beta = k_{bb1}/(k_{bb1} + k_{bb2})$).

Finally, according to the kinetic schemes of Figures 2 and 3, the concentration of long and short chain branches, LCB and SCB, respectively is given by the

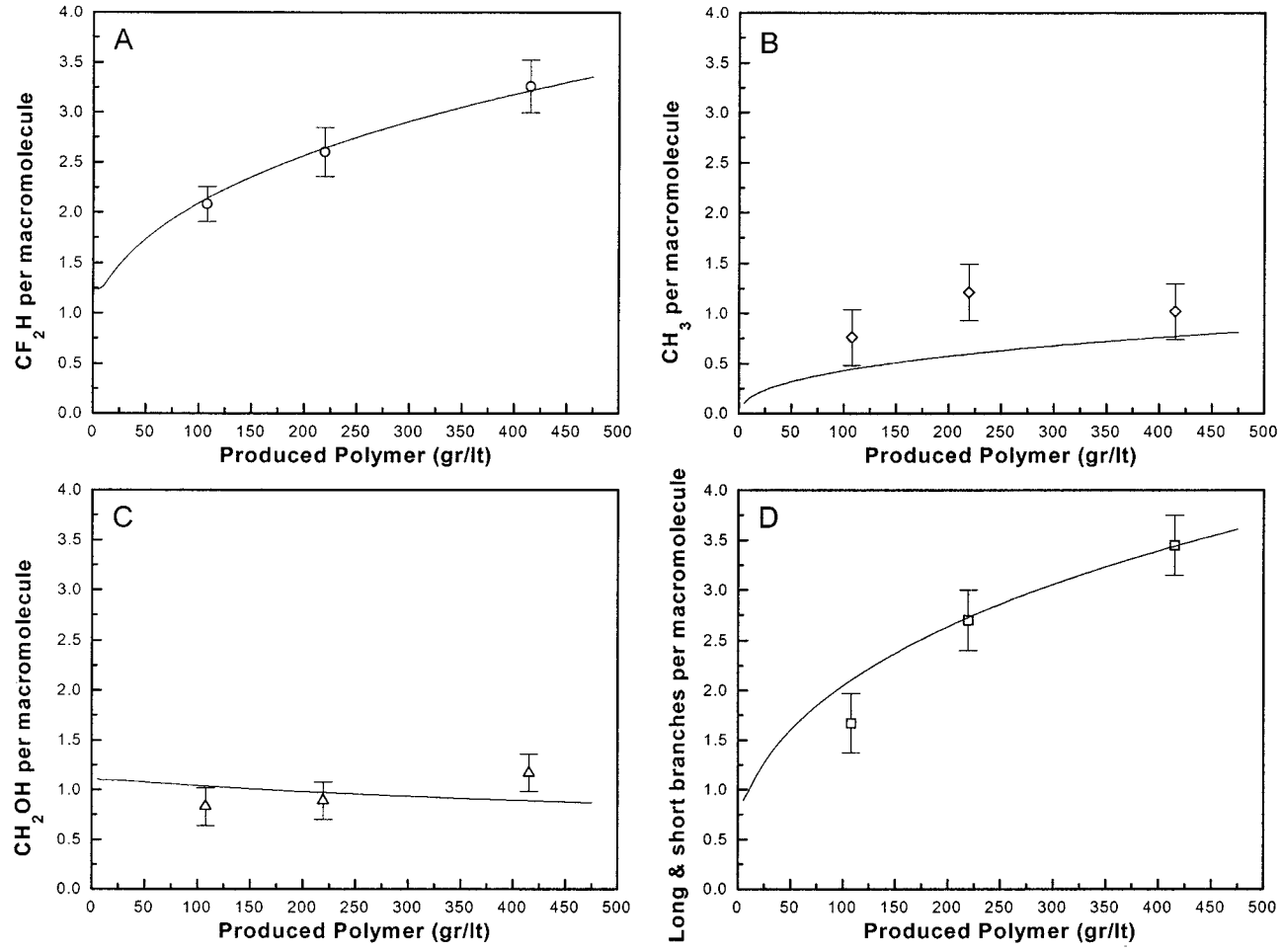

Figure 6. VDF−HFP copolymerization (runs 1−3). (A) CF_2H per polymer chain as a function of the polymer produced. Solid line: model prediction. Circles: experimental data from NMR measurements. (B) CH_3 per polymer chain as a function of the polymer produced. Solid line: model prediction. Diamonds: experimental data from NMR measurements. (C) CH_2OH per polymer chain as a function of the polymer produced. Solid line: model prediction. Triangles: experimental data from NMR measurements. (D) Long and short branches per polymer chain as a function of the polymer produced. Solid line: model prediction. Squares: experimental data from NMR measurements.

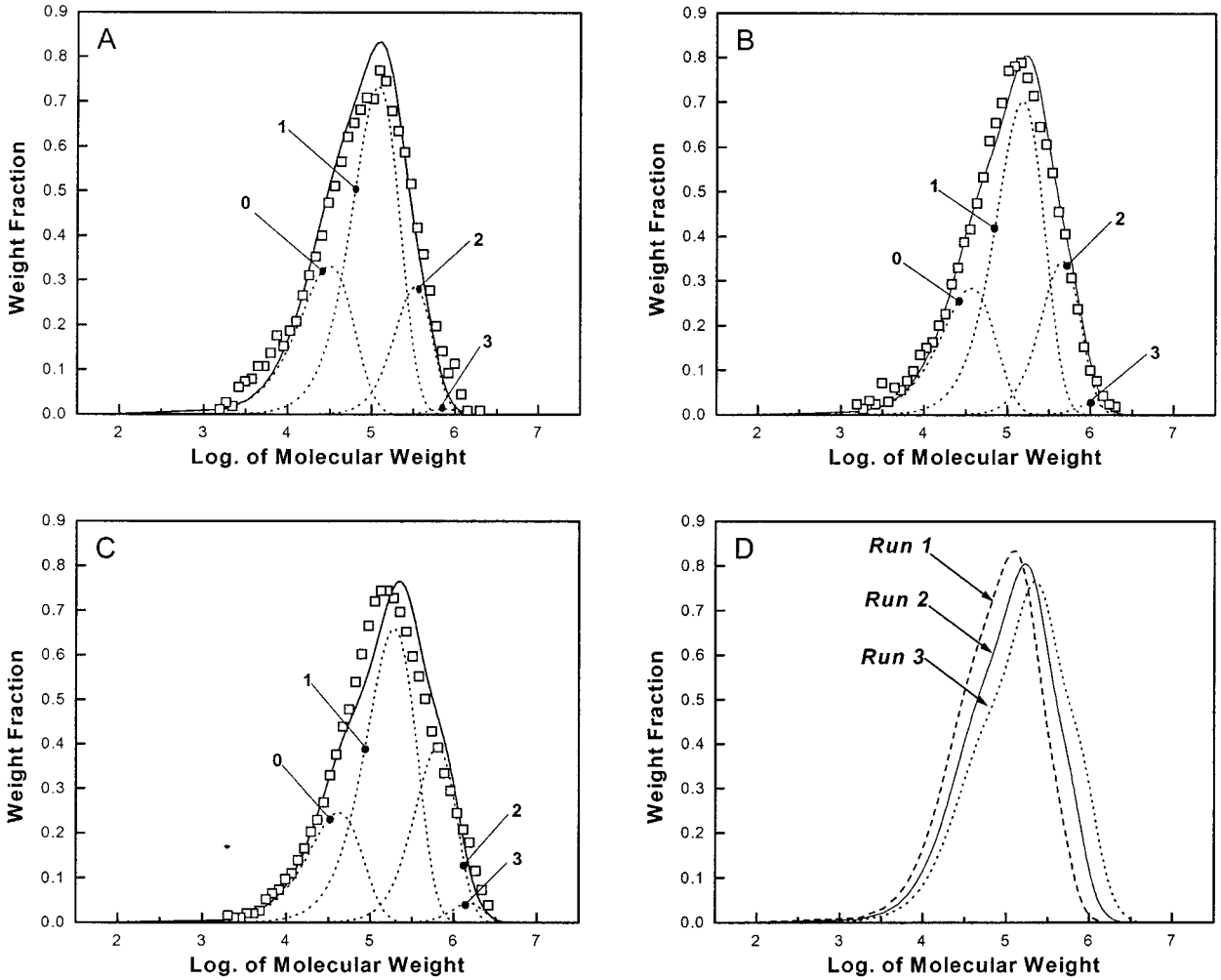

Figure 7. MWD evolution with the amount of polymer produced (runs 1−3). (A) MWD of run 1 (low conversion). Points: experimental data from GPC analysis. Solid line: calculated MWD. Dotted lines: MWD of each polymer generation. (B) MWD of run 2 (medium conversion). Points: experimental data from GPC analysis. Solid line: calculated MWD. Dotted lines: MWD of each polymer generation. (C) MWD of run 3 (high conversion). Points: experimental data from GPC analysis. Solid line: calculated MWD. Dotted lines: MWD of each polymer generation. (D) Comparison between the calculated MWD of runs 1−3.

following equations:

$$\frac{\mathrm{d(LCB)}}{\mathrm{d}M_c} = C_{fp}\frac{Q_1}{M} + C_p^*\alpha\frac{Q_0}{M} \tag{39}$$

$$\frac{\mathrm{d(SCB)}}{\mathrm{d}M_c} = C_{bb}\frac{1}{M}\frac{V_p}{V_w} \tag{40}$$

where it is seen that chain transfer to polymer and propagation to TDB reactions generate LCBs, while backbiting produces SCBs.

3. Estimation of the Model Parameters

3.1. Independent Literature Sources. Some of the physicochemical parameters used in the model have been evaluated based on independent literature information as reported in Table 2, where the corresponding literature sources are also indicated. The values of Henry's constants have been measured at reaction temperature and pressure by solubility measurements in exhausted latexes for each pure monomer. It is worth noticing that the knowledge of reactivity ratios and monomer concentrations in the polymer particles, which are given in this table, are sufficient to evaluate the evolution of polymer composition as a function of conversion.

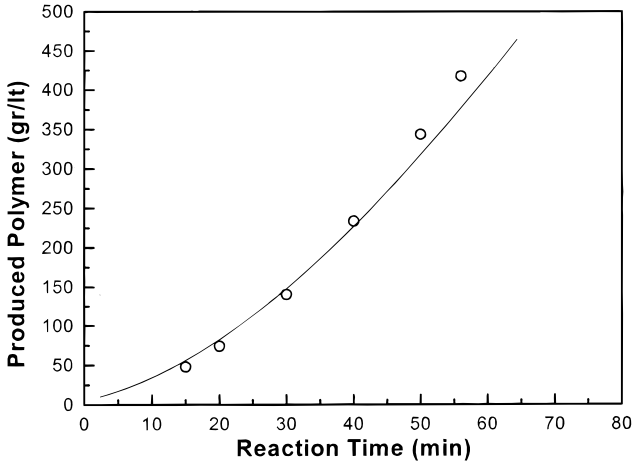

Figure 8. Polymer produced as a function of time for run 4. Solid line: model prediction. Circles: experimental data.

3.2. Fitting of Experimental Data. Because of the lack of kinetic data relative to the emulsion polymerization of fluorinated monomers in the open literature, most of the model kinetic parameters have been evaluated by fitting the experimental data reported in this

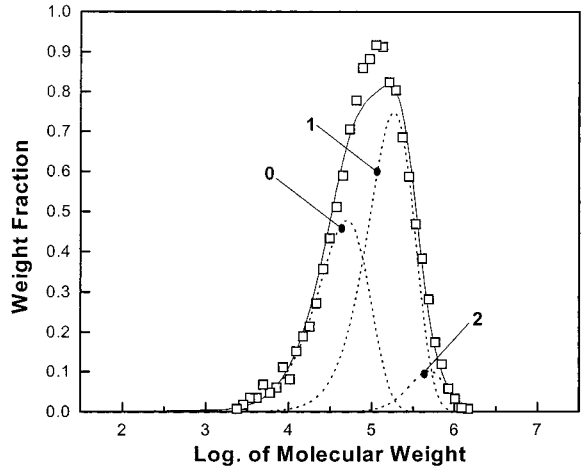

Figure 9. MWD for run 4. Squares: experimental data from GPC analysis. Solid line: calculated MWD. Dotted lines: MWD of each polymer generation.

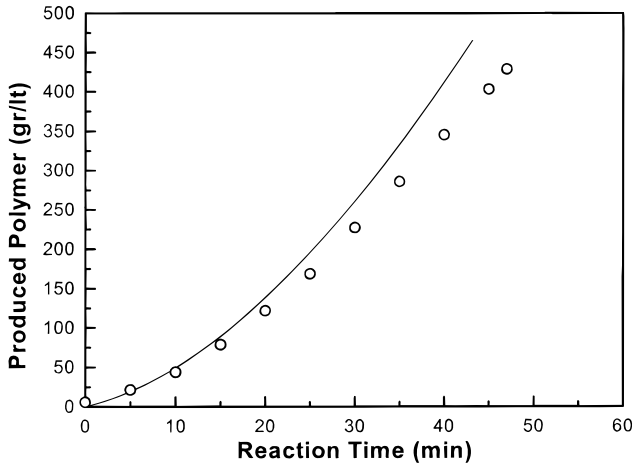

Figure 10. Polymer produced as a function of time for run 5. Solid line: model prediction. Circles: experimental data.

work. In particular, to evaluate the kinetic parameters of the model, two "reference" copolymerization reactions (the first one repeated three times and stopped at different conversion values) have been carried out. The polymerization recipes are summarized in Table 1 (runs 1−3 and 4) while the experimental procedure has been described in section 1.1. It should be noted that although the model parameters are many, the estimation procedure remains well-balanced because of the rather detailed characterization of the polymer chains that has been performed. Thus, by fitting the model results to the data of conversion, MWD and chain end group concentrations measured in the experiments without CTA (runs 1−3), the values of all the kinetic parameters but C_{ft} have been first obtained. Then, the value of the chain-transfer ratio C_{ft} has been estimated by fitting the data of run 4. The resulting set of model parameter values is summarized in Table 3. Let us now analyze in some more details the results obtained for these two sets of operating conditions.

3.2.1. Reactions without a Chain-Transfer Agent (Runs 1−3). The reaction evolution in the absence of CTA (runs 1−3) is shown in Figure 4, where the calculated conversion values are compared to the experimental data as a function of time. Note that the experimental data have been obtained by monomer feed flow rate measurements. The data in Figure 4 belong to the same experiment repeated three times (runs 1−3)

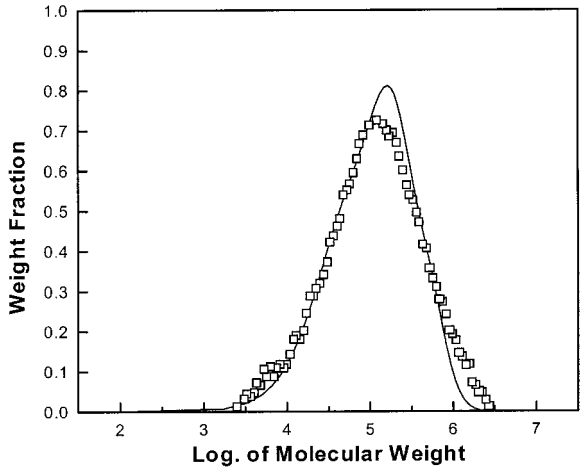

Figure 11. MWD for run 5. Squares: experimental data from GPC analysis. Solid line: calculated MWD.

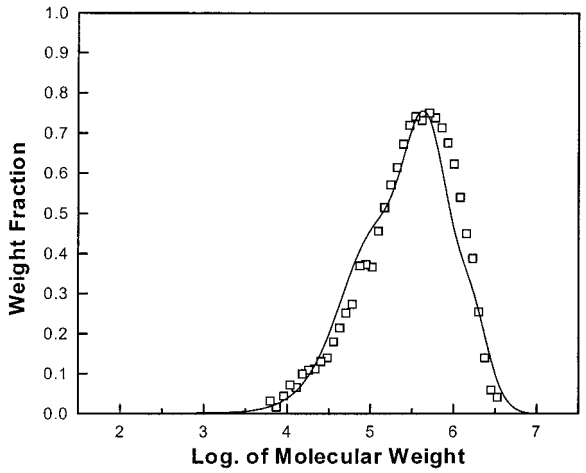

Figure 12. MWD for run 6. Squares: experimental data from GPC analysis. Solid line: calculated MWD.

and then indicate not only a good fit with the model results but also a good reproducibility of the experiments.

About the polymer chain structure, in Figure 5, parts A and B, is shown the evolution with conversion of the number-average molecular weight, M_N, and the polydispersity index, P_d. The increase of the average chain length shown in Figure 5A is due to the presence of long-chain branching. In fact, since the polymerization reaction is carried out at constant pressure, the monomer concentration in the polymer particles remains constant. In these conditions, only a chain reactivation mechanism can explain increasing molecular-weight values, and this leads also to long-chain branching. From the results shown in Figure 5C we see that indeed long-chain branches are present, although to a modest extent (i.e., about 1.5 branches/chain).

Finally, let us comment briefly on the reliability of the adopted numerical technique based on numerical fractionation as discussed above. In Figure 5D, the polydispersity indexes for each polymer generation at final conversion are shown. It appears that P_d is always relatively small (i.e., lower than 2.3) and decreases toward 1 as the generation index increases. This observation indicates that the adopted fractionation rules succeeded in dividing the overall population of polymer chains (whose final polydispersity value is larger than 5) into generations of macromolecules with relatively

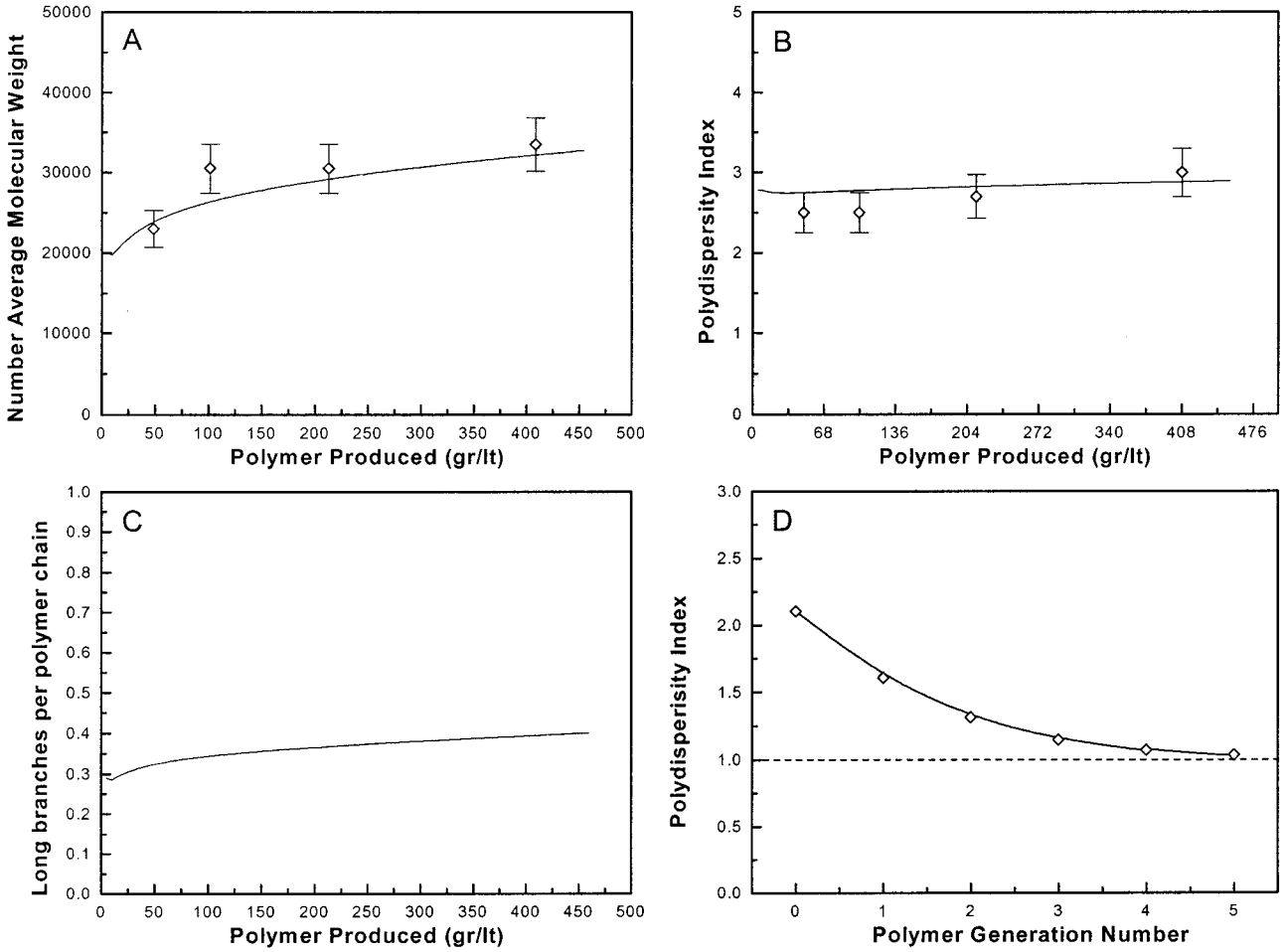

Figure 13. VDF−HFP copolymerization (runs 7−10). (A) Number-average molecular weight as a function of the polymer produced. Solid line: model prediction. Points: experimental data from GPC measurements. (B) Polydispersity index as a function of the polymer produced. Solid line: model prediction. Points: experimental data from GPC measurements. (C) Calculated long-chain branches per macromolecule as a function of the polymer produced. (D) Calculated polydispersity index of the MWD for each polymer generation.

similar chain lengths. This also justifies the use of only the first three moments to calculate the MWD for each generation.

In Figure 6, parts A−C, the calculated number of chain end groups of type CF_2H, CH_3, and CH_2OH are compared to the experimental data measured through NMR as a function of conversion. Further, in Figure 6D the average number of long and short branches per macromolecule computed by the model through eqs 39 and 40 are compared to the corresponding experimental values obtained as described in subsection 1.3. It is worth noting that NMR cannot measure the TDB chain end because the corresponding peak is not resolved, and therefore it has been excluded from this comparison. From the model simulations, we have seen that the average number of TDB per polymer chain remains almost constant and equal to about 0.5 through the entire polymerization reaction.

Finally, let us consider the model−experiment comparison in terms of the entire MWD as illustrated in Figure 7. In particular, Figure 7, parts A−C, shows the MWDs at three different (increasing) conversion values. In Figure 7D, the three curves are superimposed to show the drift of the MWD toward higher molecular weights. Note that the solid line in the first three figures indicates the computed overall MWD while the dotted curves represent the MWD of the different polymer generations. The digits indicate the generation order. It is seen that increasing order generations correspond to increasing molecular weights. The observation of the MWDs relative to the single generation provides some physical insights about the evolution of the polymerization reaction. In particular, we note that the fraction of chains in the 0th-order generation decreases with conversion, while that in the third generation increases (see the areas below the distributions). This is due to the two branching mechanisms indicated in the kinetic scheme of Figure 3 (i.e., chain transfer to polymer and propagation to TDB reactions). Under the reaction conditions of runs 1−3, these two mechanisms do not lead to gel formation and four generations are sufficient to describe the overall MWD. It is worth noting that the simulations were performed using six generations but the amount of polymer in the fifth and sixth generations was found to be negligible. On the other hand, the first generation (the first after the linear one) is the most abundant in terms of weight fraction, thus indicating that most of the chains are branched. This rather unexpected result (the rate of the reactions producing branching are in fact relatively small for this system, cf. Table 3) is justified by the large polymer-to-monomer ratio inside the particles, because of the very small solubilities of the monomers in the copolymer.

3.2.2. Reaction with a Chain-Transfer Agent (Run 4). To estimate the rate coefficient of the chain

transfer reaction to CTA (i.e., ethyl acetate), run 4 was carried out and the MWD of the obtained polymer was measured. By fitting the model predictions to the experimental data, the C_{ft} value reported in Table 3 was determined. The results of the best fit are shown in Figures 8 and 9 in terms of conversion as a function of time and final MWD, respectively. In both cases the agreement is satisfactory. It is found that, as expected, the presence of a CTA greatly reduces the polymer molecular weight as well as the number of branches per macromolecule. This is evident also from the results of numerical fractionation shown in Figure 9, where it appears that the first three polymer generations are sufficient to accurately describe the overall MWD of the polymer.

4. Experimental Validation of the Model

After having estimated all the model parameters by fitting a set of experimental data as shown in the previous section (Tables 2 and 3), we now proceed to assess the model capability of predicting the system behavior at different operating conditions. This is done in this section by comparing the model predictions to a new set of experimental data. In particular, six polymerization reactions have been carried out: the effects of initiator concentration and of reactor pressure are investigated in runs 5 and 6, respectively, while the effect of CTA concentration has been studied at four different conversion levels in runs 7−10.

4.1. Effect of Initiator Concentration. Run 5, the same recipe as that in runs 1−3 but with a double initial initiator concentration (cf. Table 1), has been considered. The system behavior is compared in Figure 10 to the model prediction in terms of the polymer produced as a function of time.

The MWD measured at the end of the polymerization is compared to that predicted by the model in Figure 11. On the whole, the model performance appears to be satisfactory. It is worth noting, by comparing Figures 11 and 7C, that the MWD is slightly affected by the initiator concentration. This is a consequence of the small effect of the termination mechanisms involving two radicals on the polymer chain length, which is instead controlled by chain transfer to monomer and to polymer reactions. The effect of the initiator in accelerating the polymerization rate is instead significant, as shown by the comparison between Figures 4 and 10.

4.2. Effect of Pressure. To investigate the effect of reaction pressure on the MWD of the polymer produced, the experimental run 6 has been carried out at a pressure larger than that in runs 1−3 (i.e., 1.1 vs 1.9 MPa, cf. Table 1). In this experiment, the initiator concentration has been reduced to $^1/_3$ of the concentration of runs 1−3. Therefore, the pressure effect examined here is combined with that of the initial amount of initiator. Since, as observed above, the initiator concentration in this system has a minor effect on the MWD, the observed changes should be attributed to the increased pressure value.

The comparison between calculated and experimental MWDs is shown in Figure 12. It is worth noting that the molecular weight of the polymer produced in run 6 (M_N = 115 000 kg/kmol) is much larger than that of the base case, run 3 (M_N = 47 000 kg/kmol), although the same value of conversion was achieved in the two experiments. This behavior is due to the increase of monomer concentration in the polymer particles and is

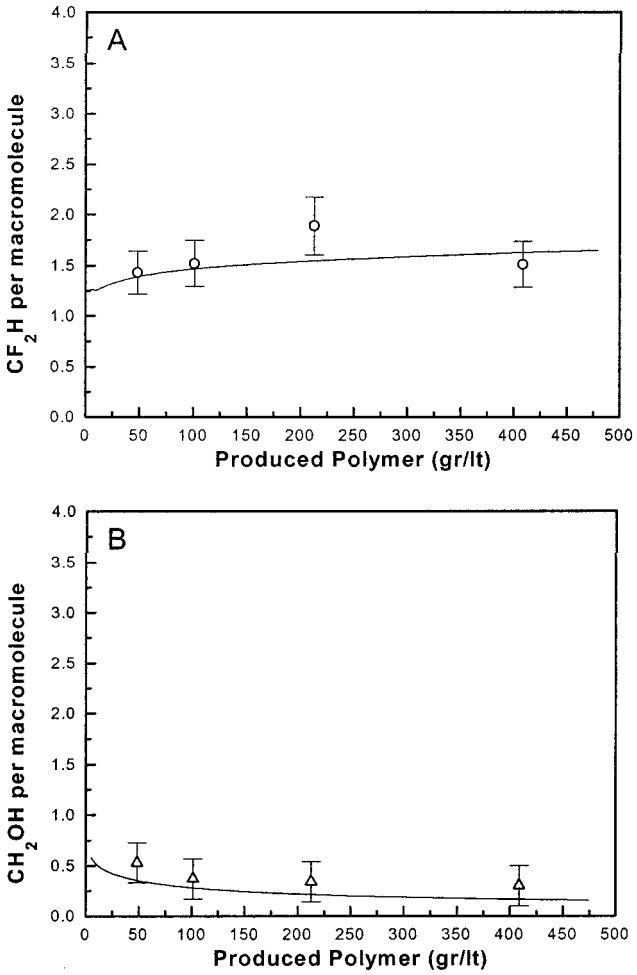

Figure 14. VDF−HFP copolymerization (runs 7−10). (A) CF_2H per polymer chain as a function of the polymer produced. Solid line: model prediction. Circles: experimental data from NMR measurements. (B) CH_2OH per polymer chain as a function of the polymer produced. Solid line: model prediction. Triangles: experimental data from NMR measurements.

correctly predicted by the model. The shoulder arising in the calculated distribution is due to the increasing weight of the generation of the linear chains with respect to those of the branched polymer. This reflects the increasing probability of chain propagation with respect to that of branching reactions when increasing the pressure (i.e., monomer concentration in the reaction locus).

4.3. Effect of the Chain-Transfer Agent (CTA). To better analyze the role of CTA, four reactions have been carried out with the same recipe, which includes a large initial concentration of ethyl acetate, but at different conversion values (runs 7−10 in Table 1).

The evolution of the number-average molecular weight with conversion is illustrated in Figure 13A. By comparing these values to those in Figure 5A, obtained without CTA, it appears that the use of a CTA greatly reduces the drift of the molecular weight with conversion. This is also due to the large water solubility and low reactivity of ethyl acetate, which made its concentration in the polymer particles substantially constant throughout the entire polymerization reaction. A constant CTA concentration leads to instantaneous MWDs which remain uniform during the process. In addition, the presence of CTA significantly reduces the effect of the branching mechanisms on the MWD. Accordingly, the

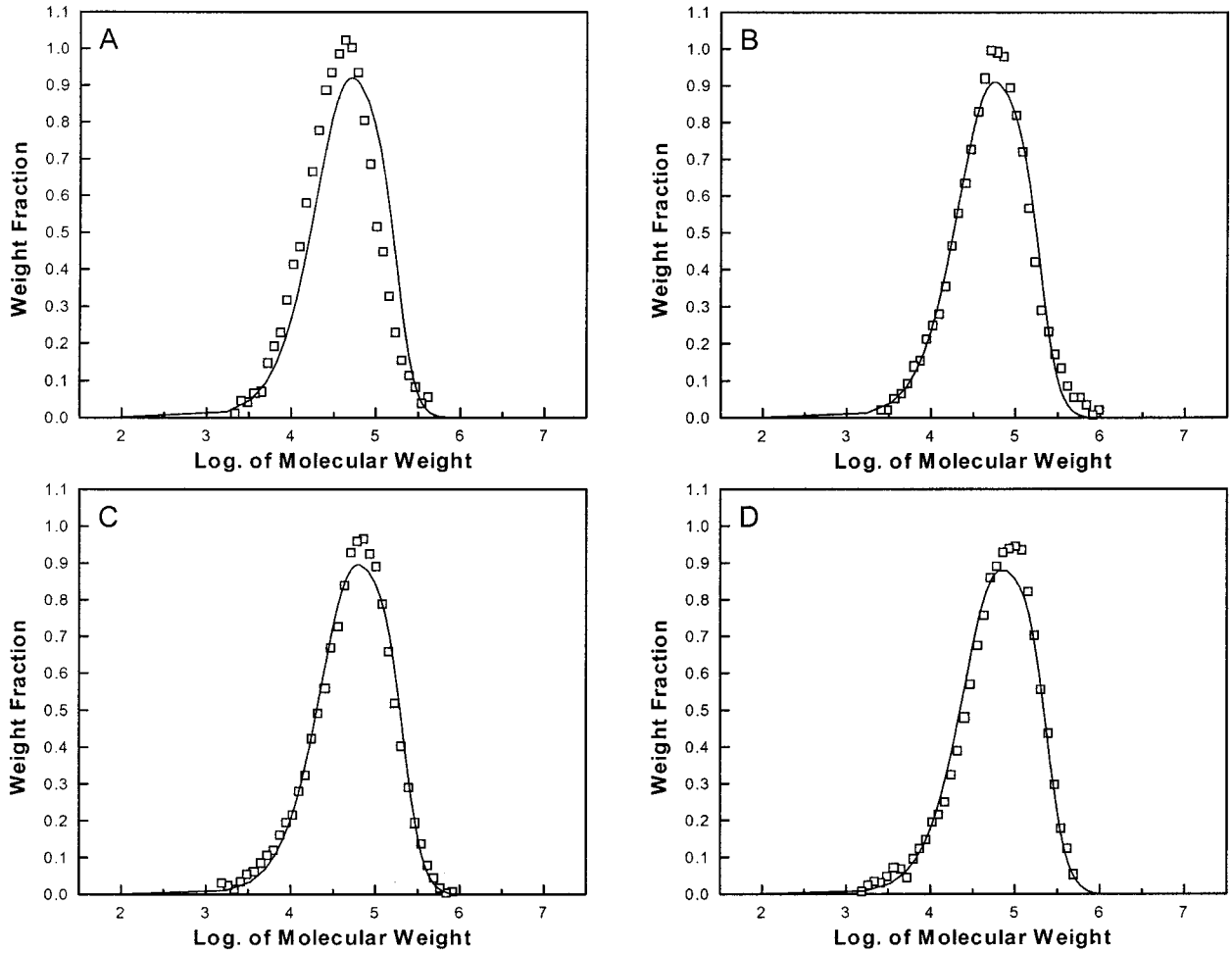

Figure 15. MWD evolution as a function of the polymer produced for runs 7−10. (A) MWD of run 7 (very low conversion). Squares: experimental data from GPC analysis. Solid line: calculated MWD. (B) MWD of run 8 (low conversion). Squares: experimental data from GPC analysis. Solid line: calculated MWD. (C) MWD of run 9 (medium conversion). Squares: experimental data from GPC analysis. Solid line: calculated MWD. (D) MWD of run 10 (high conversion). Squares: experimental data from GPC analysis. Solid line: calculated MWD.

polydispersity index is significantly reduced and remains constant during polymerization, as shown in Figure 13B. On the other hand, in Figure 13C it is seen that the number of long-chain branches per molecule is rather low (≤ 0.5) even at high conversion. This behavior is reflected also by the numerical fractionation method which predicts rather narrow MWD for all polymer generations, with a polydispersity index value which is never greater than 2.1, as shown in Figure 13D. This makes this discretization technique particularly effective in the case under examination.

The CF_2H and CH_2OH chain end concentrations are shown as a function of the polymer produced in Figure 14, parts A and B, respectively. By comparison to the corresponding quantities measured in the absence of a CTA (Figure 6, parts A and C), it readily appears that the relative concentration of CF_2H with respect to CH_2OH is significantly increased. This confirms the dominant role of chain transfer to the CTA as the chain-initiating mechanism compared to initiator decomposition.

Finally, the evolution of the MWD with the amount of polymer produced is shown in Figure 15. Besides the satisfactory agreement between model predictions and experimental measurements, it appears that the MWD remains substantially unaltered during polymerization.

5. Conclusions

In this work, the free-radical emulsion copolymerization of vinylidene fluoride and hexafluoropropylene has been investigated. Despite its increasing importance in the polymer industry, the polymerization kinetics of this system is largely unknown and very few data are available in the open literature. A reliable kinetic scheme for the VDF−HFP copolymerization has been formulated and an efficient procedure to estimate all the involved kinetic parameters has been developed. The adopted procedure, based on a rather *extensive characterization* of the microstructure of a relatively *small number of polymer samples*, is summarized below.

(1) A rather detailed analysis of the chemistry of VDF−HFP polymerization has been carried out mainly based on NMR data. The most important chain end groups have been determined and, on the basis of mechanistic considerations, a reasonable reaction scheme has been derived. This information is well-representative of the effect of each of the reactions in the kinetic mechanism and therefore allows a reliable estimation of the corresponding kinetic parameters to be made. This is largely due to the chain end group distribution, which really provides a sort of fingerprint of the set of termination reactions acting in the system.

(2) The reaction scheme has been used to develop a mathematical model for calculating the MWD as well

as the chain end distribution of the produced polymer. Since the VDF−HFP copolymer is branched, sometimes, depending upon the polymerization condition, polymer gel fractions can be produced. The evaluation of the MWD in these cases is not trivial and it has been done using the numerical fractionation technique.

(3) To estimate the model kinetic parameters, a first set of experimental data has been used. By fitting the model results to the experimental data (polymerization rate, MWD, and chain end group distribution), an estimate of all the kinetic parameters of VDF−HFP free-radical polymerization has been obtained.

(4) The reliability of the model has been tested with a second and independent set of experimental data. In this case, different conditions have been investigated, such as pressure, initiator concentration, and chain-transfer agent concentration.

In general, the agreement between model predictions and experimental data is fairly satisfactory, thus confirming the accuracy of the proposed approach. In this connection, particularly significant is the accuracy in the prediction of the MWD of the VDF−HFP copolymer since branched macromolecules are involved.

Finally, it is worth mentioning that the mathematical model developed here is based on a set of ordinary differential equations whose solution requires less than 5 min on a standard personal computer. This makes the model particularly suitable to design polymers with a tailor-made microstructure.

References and Notes

(1) Ram, A.; Miltz, J. *J. Appl. Polym. Sci.* **1971**, *15*, 2639.
(2) Pianca, M.; Tatò, M.; Del Fanti, N.; Moggi, G. Ausimont Internal Report No. 57/86, Ausimont R&D: Bollste, Italy, 1986.
(3) Xie, T.; Hamielec, A. E. *Makromol. Chem., Macromol. Symp.* **1993**, *2*, 455.
(4) Storti, G.; Carrà, S.; Morbidelli, M.; Vita, G. *J. Appl. Polym. Sci.* **1989**, *37*, 2443.
(5) Apostolo, M.; Storti, G.; Morbidelli, M. Microstructure of fluorinated Monomers: A Mathematical Model, poster presented at North American Research Conference on the Science and Technology of Emulsion Polymers/Polymer Colloids, ACS—The Division of Polymeric Materials. Science and Engineering, Hilton Head Island, SC, Nov 6−8, 1995.
(6) Mayo, F. R.; Lewis, F. M. *J. Am. Chem. Soc.* **1944**, *66*, 1594. Alfrey, T.; Goldfinger, G. *J. Chem. Phys.* **1944**, *12*, 205.
(7) Martin, J. J. *Ind. Eng. Chem. Fundam.* **1979**, *18*, 81.
(8) Zhu, S.; Hamielec, A. E. *J. Polym. Sci., B: Polym. Phys.* **1994**, *32*, 929.
(9) Fiorentino, S.; Ghielmi, A.; Storti, G.; Morbidelli, M. *Ind. Eng. Chem. Res.* **1997**, *36*, 1283.
(10) Tatemoto, M. In *Proceedings of IX International Symposium on Fluorine Chemistry*; Daikin Koygo Co., Ltd.: Osaka, Japan, 1979.
(11) Logothetis, A. *Prog. Polym. Sci.* **1989**, *14*, 251.
(12) Xie, T.; Hamielec, A. E. *Makromol. Chem., Macromol. Symp.* **1993**, *2*, 421.
(13) Ray, W. *J. Macromol. Sci.—Rev. Macromol. Chem.* **1972**, *C8*, 1.
(14) Lowry, G. G. *Markov Chains and Monte Carlo Calculation in Polymer Science*; Marcel Dekker: New York, 1970.
(15) Lichti, G.; Gilbert, R. G.; Napper, D. H. *J. Polym. Sci., Polym. Chem. Ed.* **1980**, *18*, 1292.
(16) Tobita, H.; Takata, Y.; Nomura, M. *Macromolecules* **1994**, *27*, 3804.
(17) Storti, G.; Polotti, M.; Cociani, M.; Morbidelli, M. *J. Polym. Sci., A: Polym. Chem.* **1992**, *30*, 731.
(18) Bamford, C. H.; Tompa, H. *J. Polym. Sci.* **1953**, *10*, 345.
(19) Tobita, H.; Ito, K. *Polym. React. Eng.* **1992−93**, *1*, 407.
(20) Flory, P. J. *J. Am. Chem. Soc.* **1941**, *63*, 3083, 3091, 3096.
(21) Stockmayer, W. H. *J. Chem. Phys.* **1943**, *11*, 45.
(22) Stockmayer, W. H. *J. Chem. Phys.* **1944**, *12*, 125.
(23) Tobita, H.; Hamielec, A. E. *Macromolecules* **1989**, *22*, 3098.
(24) Zhu, S.; Hamielec, A. E. *Makromol. Chem., Macromol. Symp.* **1992**, *63*, 135; **1993**, *69*, 247.
(25) Wulkow, M. *Macromol. Theory Simul.* **1996**, *5*, 393.
(26) Fiorentino, S.; Ghielmi, A.; Storti, G.; Morbidelli, M. *Ind. Eng. Chem. Res.* **1997**, *36*, 1283.
(27) Teymour, F.; Campbell, J. D. *Macromolecules* **1994**, *27*, 2460.
(28) Arzamendi, G.; Asua, J. M. *Macromolecules* **1995**, *28*, 7479.
(29) Ghielmi, A.; Fiorentino, S.; Storti, G.; Mazzotti, M.; Morbidelli, M. *J. Polym. Sci., A: Polym. Chem.* **1997**, *35*, 827.
(30) Dotson, N. A.; Galvan, R.; Laurence, L. R.; Tirrell, M. In *Polymerization Process Modeling*; VCH Publishers Inc.: New York, 1996; p 45.
(31) Hulburt, H. M.; Katz, S. *Chem. Eng. Sci.* **1964**, *19*, 555.
(32) Apostolo, M. Ausimont Internal Report No. 1/97, Ausimont R&D: Bollste, Italy, 1997.

MA980683R